JOURNAL OF Materials CHEMISTRY

Electronic structure and stability of the $Li_xMn_2O_4$ ($0 < x < 2$) system

Helena Berg,* Kenneth Göransson, Bengt Noläng and John O. Thomas

Inorganic Chemistry, Ångström Laboratory, Uppsala University, Box 538, SE-751 21 Uppsala, Sweden. E-mail: helena.berg@kemi.uu.se

Received 12th July 1999, Accepted 20th August 1999

LMTO-ASA self-consistent band structure calculations have been performed for the cubic spinel $LiMn_2O_4$ and its delithiated and lithiated phases: λ-MnO_2 and $Li_2Mn_2O_4$. It has been shown that the Jahn–Teller distortion plays a vital rôle in the stabilisation of the $Li_2Mn_2O_4$ phase. The influence on the band structure of different possible positions for the lithium ions is investigated, and the phase transition from cubic to tetragonal symmetry for $Li_2Mn_2O_4$ discussed. The *change* in potential associated with the insertion of lithium ions into λ-MnO_2 to form $LiMn_2O_4$ and $Li_2Mn_2O_4$ has been calculated as 1.51 V and 1.16 V, respectively. The lithium atoms are ionised by contributing substantial character to the bonding band. However, the charge transfer is small and the electron density around the lithium ions is higher than in lithium metal.

Introduction

One of the major challenges in the development of improved rechargeable lithium–polymer batteries is the discovery of new electrode materials which can serve as hosts for lithium-ion insertion. Current technology uses transition-metal oxides, which serve as high-performance cathode materials.[1–4] The ideal oxide must have high operating voltage, high capacity and be cyclable. $LiCoO_2$ is currently the most favoured positive electrode.[5,6] However, its high cost and unacceptable level of toxicity have motivated extensive interest in $LiMn_2O_4$ as a cathode material over the past decade,[7–10] in spite of its lower theoretical capacity: 148 mA h g^{-1} compared to 275 mA h g^{-1} for $LiCoO_2$. In practice, however, the accessible capacities of the two compounds are almost equal, since lithium ions are not totally extractable from $LiCoO_2$. The lower cost and non-toxicity of $LiMn_2O_4$ thus make it a most attractive candidate for further study.

$LiMn_2O_4$ crystallises in the spinel structure, and the arrangement of manganese and oxygen atoms can be seen as a three-dimensional framework for an interlinked network of tetrahedral and octahedral interstices, which can serve as pathways for the transport of lithium ions. The manganese/oxygen framework remains essentially the same for lithium insertion/extraction processes in the composition range $Li_xMn_2O_4$, $0 \leqslant x \leqslant 2$. This paper presents calculations of the electronic structures of the $Li_xMn_2O_4$ system for the cases $x = 0$, 1 and 2, using the Linear Muffin-Tin Orbital method in the Atomic Sphere Approximation (LMTO-ASA). A number of quantities are derived: electron densities, orbital occupancies, densities of states, band-gaps, and the average operating voltages for lithium-ion insertion. The relative stabilisation energies associated with the four possible lithium positions are compared, and the phase transition from cubic to tetragonal symmetry, occurring on lithium-ion insertion into $LiMn_2O_4$, is discussed. Previous calculations of the electronic structure of lithium intercalation compounds have generally involved rigid-band and semi-empirical tight-binding methods.[11–15] These methods can, at best, provide only a qualitative understanding of electronic structure. More accurate calculations, using linear augmented plane-wave (LAPW) and LMTO-ASA have been performed for TiS_2 and $LiTiS_2$.[16,17] Aydinol *et al.*[18] have made more accurate calculations using the *ab initio* pseudopotential method for a number of metal oxides with composition $LiMO_2$ (M = Ti, V, Mn, Co, Ni, Cu, Zn and Al) all of which have the α-$NaFeO_2$ structure. The cases involving Mn, Ti, and Zn are not stable in this structure, and the series studied illustrates the changes in electronic structures as a function of the position of the metal in the periodic system, rather than describing the properties of a particular compound. In other work,[19] the same method has been exploited for more detailed calculations on $LiMn_2O_4$ and $Li_2Mn_2O_4$. A limitation of the $Li_2Mn_2O_4$ calculation, however, was that it was made for an idealised cubic structure with the lithium atoms occupying only one type of site, and not for the experimentally observed tetragonally distorted structure with lithium atoms occupying two different types of position.[10,20] The accuracy of the calculations was also low since they used only a minimum set of *k*-points.

In this present work, both the tetragonal distortion and different types of lithium positions have been taken into account by using LMTO-ASA calculations for a large number of *k*-points. These calculations allow us to separate the effects of the tetragonal distortion and the different lithium-atom positions. Their relative importance in determining the lithium intercalation voltage can thus be deduced; this is an issue which has been discussed extensively in earlier work.[18,19]

The crystal structures

$LiMn_2O_4$ crystallises in the cubic spinel structure with space group *Fd*3*m*, $Z = 8$. The unit cell thus contains 56 atoms: 8 Li, 16 Mn and 32 O. The crystal structure can be described as a closed-packed array of oxygen atoms (32e positions) with lithium atoms occupying tetrahedral 8a positions and manga-

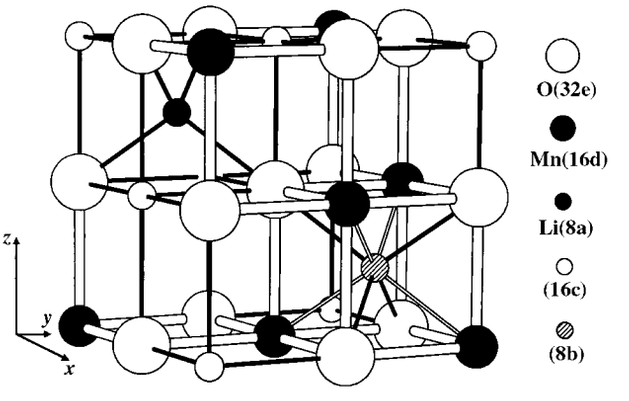

Fig. 1 A part of the cubic $LiMn_2O_4$ spinel structure (space group: *Fd*3*m*).

nese atoms octahedral 16d positions in the oxygen framework (Fig. 1). The octahedral arrangement of oxygen atoms around manganese is slightly distorted; the oxygen-atom coordinate (x, x, x) has been determined by neutron powder diffraction as 0.2632(2);[7] *ca.* 0.2 Å displaced from the special position at (¼, ¼, ¼).

Lithium ions can be extracted from $LiMn_2O_4$ to form the λ-MnO_2 phase, while still maintaining cubic symmetry.[21] Lithium-ion insertion into λ-MnO_2 causes the cell to expand isotropically up to the composition $Li_{1.08}Mn_2O_4$.[20] Further lithium-ion insertion is known to result in the creation of high-spin Mn^{3+} ions with accompanying Jahn–Teller distortion and a transition from cubic to tetragonal point symmetry at the Mn^{3+} ions. Lithium atoms can then be taken up by the resulting tetragonal structure up to the composition $Li_2Mn_2O_4$.

$Li_2Mn_2O_4$ is obtained during lithium insertion into $LiMn_2O_4$ and has a tetragonal structure with space group $I4_1/amd$, $Z=2$, and c/a ratio ≈ 1.64.[10,20] This phase transition is due to a Jahn–Teller effect on Mn^{3+} ions. As indicated above, the structure is thus a distorted spinel with $a_T \approx a_C/\sqrt{2}$ and $c_T \approx a_C$ (Fig. 2), with the 4a, 8c, 8d and 16h positions in the tetragonal structure corresponding to the 8a, 16c, 16d and 32e positions in the cubic structure, respectively. Half the Li(8c) atoms and all the Mn(8d) atoms are located in a *ca.* 10% elongated octahedral arrangement of O(16h) atoms; the remaining Li(4a) atoms interleave the oxygen layers, and are tetrahedrally coordinated to oxygen atoms. The O(16h) coordinates have been refined to (0, 0.487, 0.252).[20]

Calculation method

The electronic band structures and the total energy of the valence electrons were calculated using the LMTO-ASA method assuming a frozen core.[22] Combined correction terms were included, and the calculations were performed self-consistently. The computer programs used were modified versions of those developed by Skriver.[23]

Within the ASA approximation, the volume of the unit cell is separated into overlapping atomic spheres such that their volumes sum to the total volume of the unit cell. The local descriptions of the wavefunctions within the atomic spheres facilitate the calculation of partial atomic quantities. However, these quantities are strongly dependent on how the radius of the atomic sphere is chosen; meaningful comparisons can only be made when these choices are made in a consistent manner. An r_{Mn}/r_O ratio of 1.40 was chosen by matching the potentials at the atomic-sphere surfaces in the λ-MnO_2 structure. This ratio was subsequently kept fixed in all calculations. By minimising the total valence energy as a function of both r_{Li}/r_O ratio and unit-cell volume, optimised radius ratios of $r_{Li}/r_O=1.20$ for tetrahedral Li(8a) atoms and $r_{Li}/r_O=1.30$ for octahedral Li(16c) atoms were determined. Near these optimised values, the calculated energies are virtually independent of the radius-ratio parameters. An increase by *ca.* 10% of the radius ratio does not changes the significance of the calculated properties, *i.e.* the calculated energy changes by *ca.* 30 mRy (Ry = Rydberg = $E_h/2 = 2.17987 \times 10^{-18}$ J). Empty spheres[14] were introduced in all structures at unoccupied tetrahedral and octahedral positions to achieve a better description of the s orbitals of the oxygen atoms. The relative sizes of the tetrahedral and octahedral empty spheres with respect to oxygen were fixed in all calculations to 0.7 and 0.9, respectively, on the basis of geometrical considerations.

The unit-cell dimensions for the compounds were varied isotropically, and the calculated properties presented correspond to minima in the total valence electron energy. The net charge on the different atoms is calculated as the number of valence electrons on the free atom *minus* the number of valence electrons on the atom in the compound. This results in net charges which *do not* follow the normal ionic charges (+1 for H, and −2 for O, *etc.*) since the atoms of electropositive elements are much larger in LMTO-ASA calculations than the radius usually assigned to their corresponding ions. Similarly, electronegative elements are much smaller than their corresponding ions. Orbitals of s and p character were used to describe the Li and O atoms, as well as the empty spheres; d character orbitals were added for the Mn atoms. The spinel calculations were made both for an ideal spinel phase, *i.e.* with O-coordinates (¼, ¼, ¼), and using the experimentally determined coordinate (0.2632).[7] The calculations were carried out for 505 k-points in 1/48th of the Brillouin zone for the cubic spinel phases, and 585 k-points in 1/16th of the Brillouin zone for the tetragonal phase. All the calculated properties are valid at 0 K.

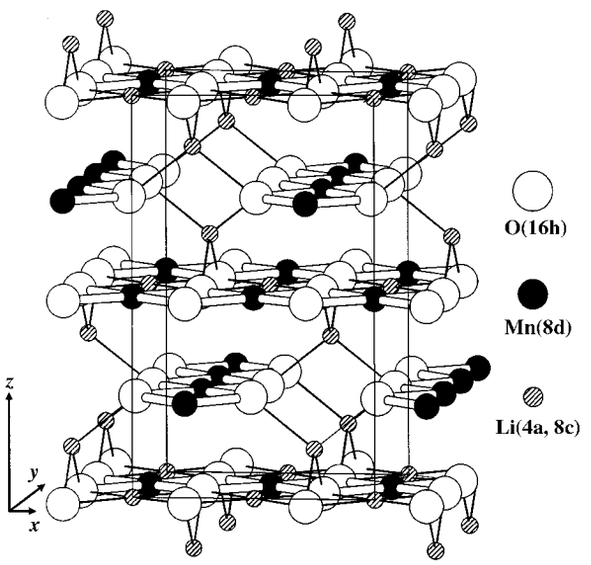

Fig. 2 The tetragonal $Li_2Mn_2O_4$ structure (space group: $I4_1/amd$).

Intercalation voltage

The open-cell voltage (OCV) between the lithium ions in a transition-metal oxide cathode and in metallic lithium depends on the chemical potential of lithium in the cathode. As lithium ions are inserted, their chemical potential in the cathode increases, leading to a decrease in OCV. Using the total valence electron energy, calculated by the LMTO-ASA method, it is possible to derive this *change* in OCV (ΔV) as a function of x in $Li_xMn_2O_4$ for perfectly ordered structures. The cell potential and the chemical potential of lithium are influenced both by short- and long-range ordering of lithium ions. Little is known about the nature of the local ordering of lithium ions in $Li_xMn_2O_4$ for $0<x<1$ and $1<x<2$. The changes in OCV have thus been calculated for the insertion limits $x=0$, 1 and 2. The change in OCV (ΔV) can be written as:

$$\Delta V(x) = -\frac{1}{F}\left(\frac{\Delta G(x)}{\delta x}\right)_{T,P} \quad (1)$$

where $\Delta G(x)$ is the change in Gibbs free energy for the reactions:

$$Li_xMn_2O_4 + \delta x Li \rightarrow Li_{x+\delta x}Mn_2O_4 \quad (2)$$

and

$$Li_{1+x}Mn_2O_4 + \delta x Li \rightarrow Li_{1+x+\delta x}Mn_2O_4 \quad (3)$$

ΔG can be separated into three terms: internal energy (ΔE), pressure–volume work ($P\Delta V$) and entropy dependence ($T\Delta S$). At 0 K, the $T\Delta S$ term is zero, and $P\Delta V$ is of the order of 10^{-5} eV. Both terms can be neglected compared to ΔE at

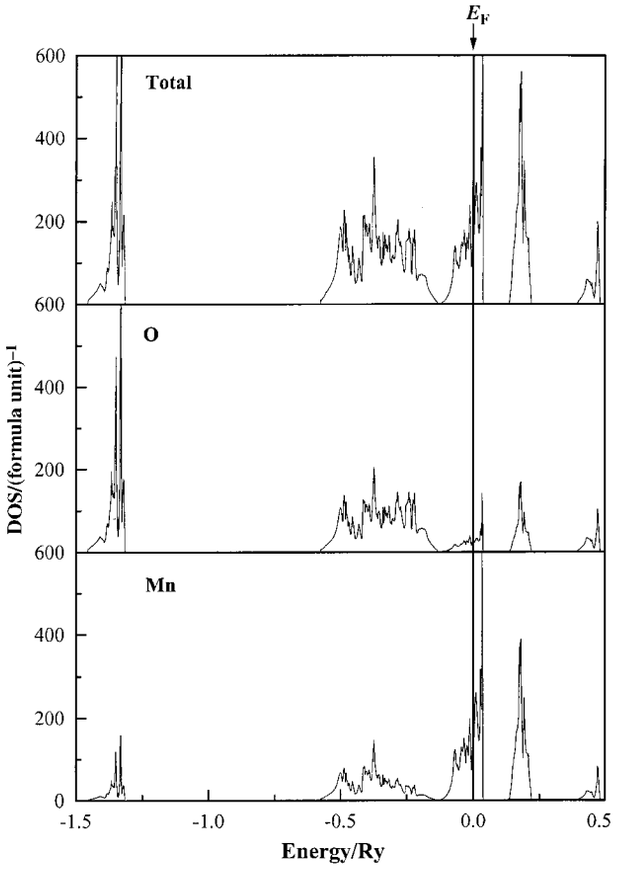

Fig. 3 Total and partial atomic density of states (DOS) for λ-MnO_2. The Fermi level has been shifted to zero. The DOS is given in units of number of states per formula unit and Rydberg (Ry).

0 K. As can be seen, the change in voltage also depends on the internal energy of metallic lithium (the anode in the considered electrochemical cell).

Results and discussion

The basic manganese/oxygen framework for the lithium-ion insertion process is that of λ-MnO_2. The results for λ-MnO_2 are therefore presented first, followed by the results for the different degrees of lithium-ion filling of the various interstices of this structure. Conceivable positions for lithium-ion insertion are only the tetrahedral 8a and the octahedral 16c positions; this is because the lithium–manganese distance becomes too short for the 8b and the 48f positions (Fig. 1). The 8a position is surrounded by four O atoms at a distance of $a(\sqrt{3}/8)$; this corresponds to the experimentally observed form of $LiMn_2O_4$. Filling half of the octahedral 16c positions also corresponds to a composition of $LiMn_2O_4$, but this atomic arrangement has not been observed experimentally. The Li–O distance is then $a/4$. Completely filling the 16c positions gives a composition corresponding to $Li_2Mn_2O_4$, but this structure has also not been observed experimentally. The stable $Li_2Mn_2O_4$ structure is the tetragonally distorted cubic form with lithium atoms occupying all the 4a and half the 8c positions.[10,20]

Three different modifications were considered for the $Li_2Mn_2O_4$ phase: two cubic and one tetragonal. The two cubic phases involved lithium atoms at 8a+16c (50% occupancy), and 16c (100% occupancy) positions, respectively. Experimentally obtained crystallographic data were used for the tetragonal structure.[20] From these calculations it is clearly seen that the Jahn–Teller distortion stabilises the tetragonal structure.

The λ-MnO_2 phase

The calculated total electronic density of states (DOS) for λ-MnO_2 has been separated out into partial atomic contributions in Fig. 3. The origin of the different bands can be deduced from inspection of the schematic energy levels of an MnO_6 octahedron (Fig. 4a). The narrow lowest-lying band is primarily of non-bonding oxygen s character. In the −0.6 to −0.15 Ry energy range, the interactions between oxygen p orbitals and manganese s, p, and d orbitals have bonding character and correspond to the $a_{1g}{}^b$, $t_{1u}{}^b$ and $e_g{}^b$ molecular orbitals of the MnO_6 octahedron. The band located in the region of the Fermi level corresponds to the non-bonding t_{2g} band. The width of the band gives evidence of some manganese–manganese interaction. The partial orbital contributions to the DOS are shown in Fig. 4b. The number of electrons corresponding to the MnO_6 octahedron in λ-MnO_2 is 15, which leaves the t_{2g} band half-filled with 3 electrons. Manganese is thus in a '4+ state', which agrees well with the integrated number of electronic states in the three energy bands

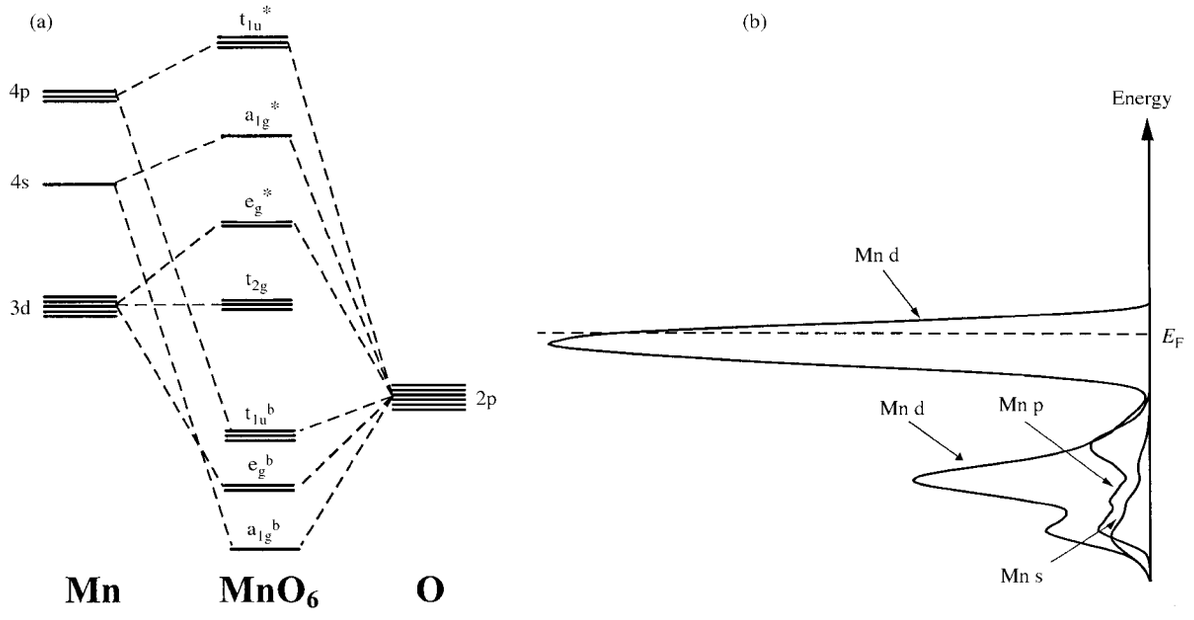

Fig. 4 Schematic splitting of the atomic orbitals for octahedral MO_6 complexes (a) and density of states (b).

Table 1 The number of states (NOS) per atomic sphere for λ-MnO_2, and for $LiMn_2O_4$ with Li occupying two types of position. The NOS has been separated into the energy intervals dominated by the indicated orbital types and atoms (E = empty sphere)

		λ-MnO_2			$LiMn_2O_4$ Li in 8a			$LiMn_2O_4$ Li in 16c		
		O s	Mn–O	Mn	O s	Mn–O	Mn	O s	Mn–O	Mn
Mn	s	0.17	0.41	0.02	0.14	0.39	0.02	0.14	0.41	0.02
	p	0.30	0.89	0.03	0.23	0.77	0.02	0.24	0.81	0.02
	d	0.29	2.09	2.93	0.23	2.20	2.98	0.25	2.15	3.04
O	s	1.58	0.04	0.01	1.61	0.02	0.00	1.62	0.03	0.00
	p	0.01	3.87	0.22	0.00	3.95	0.22	0.00	4.01	0.20
Li/E	s	0.01	0.08	0.01	0.08	0.25	0.02	0.07	0.23	0.01
(8a)	p	0.01	0.04	0.00	0.17	0.63	0.05	0.14	0.59	0.01
E	s	0.02	0.13	0.01	0.02	0.12	0.02	0.01	0.08	0.01
(tetr.)	p	0.01	0.07	0.02	0.01	0.06	0.02	0.01	0.04	0.00
E	s	0.02	0.09	0.01	0.01	0.08	0.01	0.02	0.11	0.02
(oct.)	p	0.02	0.08	0.00	0.01	0.07	0.00	0.01	0.06	0.02

presented in Table 1. However, the chemical bonding is strongly covalent, with a small ionic contribution.

In Fig. 5, the calculated electron density has been separated into the three energy intervals referred to above. The figure illustrates well the bonding/non-bonding character of the electrons in the different energy intervals. The calculated lattice parameter of 7.9215 Å (Table 2) is 1% smaller than the experimental value obtained at room temperature (not 0 K), and not for a completely lithium-free phase.[21]

The $LiMn_2O_4$ phase

The calculated total electronic DOS for the $LiMn_2O_4$ structure with lithium atoms at 8a positions and oxygen atoms at the idealised coordinates (¼, ¼, ¼), has again been separated out into partial atomic contributions in Fig. 6. The major result of lithium insertion is that the dip in the DOS between the bonding oxygen p band and the non-bonding manganese t_{2g} band develops into a pronounced gap. A small shift of the oxygen p band towards lower energies, and a small increase in the Fermi level can also be noted. The orbital character of the bonding Mn–O band in the −0.6 to −0.15 Ry range becomes an Li–Mn–O band, with Li character corresponding to approximately one electron (Fig. 6 and Table 1). Since the number of electrons in the band is constant (12) and the O character is unchanged, there is clearly a reduction of the Mn character of the band by 0.5 e−per Mn atom. This results in an increase in the Fermi level such that the non-bonding Mn t_{2g} band now contains 3.5 electrons and the Mn atoms are effectively in a '3.5+ state'. This corresponds to 15.5 electrons occupying the MnO_6 octahedron of Fig. 4. The electron of the Li atom participates strongly in the bonding and, in this sense, the Li atom is ionised. However, this does *not* mean that a charge transfer has occurred from Li to O atoms. In fact, it can be seen from Fig. 7, which plots the number of electrons within a given radius for lithium, that the number of electrons associated with the Li atom is *higher* around the Li atoms in $LiMn_2O_4$ than in b.c.c. Li metal, *i.e.* the Li 'ion' is less positive

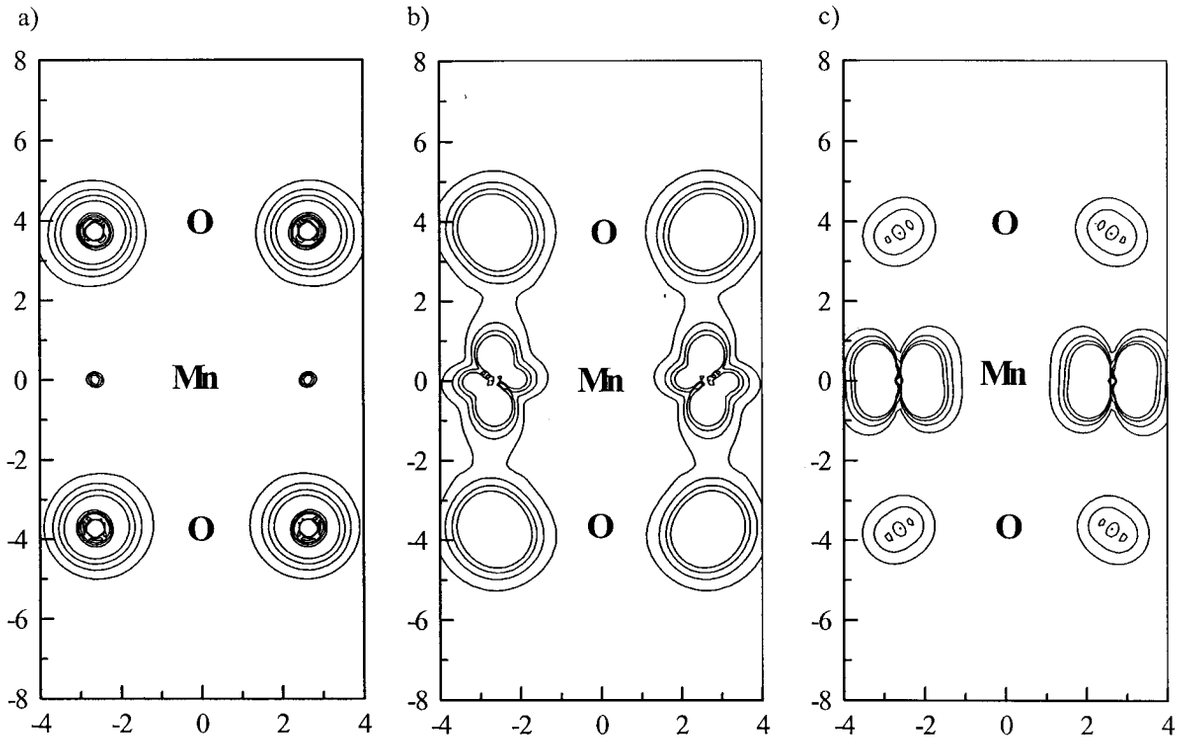

Fig. 5 The electron density in λ-MnO_2 in the (1 $\bar{1}$ 0) plane in different energy regions. (a) O s, (b) Mn–O and (c) Mn–Mn energy regions. Contour interval: 0.02 $e^- a_0^{-3}$.

Table 2 Lattice parameter (a), total valence energy/Mn (E_{tot}) for metallic lithium, and for $Li_xMn_2O_4$ ($x=0,1$ and 2) in different space groups and with lithium occupying different sites

x	Li position	O coord.	a_{calc}/Å	a_{exp}/Å	E_{tot}/Ry	Space group
0	—	¼	7.9215	8.03[a]	−96.115	*Fd*3*m*
1	8a	¼	8.1643	—	−96.338	*Fd*3*m*
1	8a	0.2632[b]	8.1643	8.251(4)[b]	−96.341	*Fd*3*m*
1	16c (50%)	¼	8.1643	—	−96.301	*Fd*3*m*
2	16c	¼	8.2476	—	−96.603	*Fd*3*m*
2	8a+16c (50%)	¼	8.3719	—	−96.540	*Fd*3*m*
2	4a+8c (50%)	[c]	$a=5.6431$ $c=9.2430$	5.662(2)[c] 9.274(4)[c]	−96.652	$I4_1/amd$
Li	2a	—	3.4212	3.510[d]	−0.282	*Im*3*m*

[a]Ref. 21. [b]Ref. 7. [c]Ref. 20. [d]PDF-file 15-0401.

in $LiMn_2O_4$ than in Li metal. The net charge on the lithium atom is −0.21 for an atomic sphere radius of 1.27 Å. The number of electrons within a radius of 0.59 Å[24] (that usually assigned to Li^+ ions in tetrahedral coordination) corresponds to a net charge of +0.93 and +0.97 for the lithiated phase and lithium metal, respectively. The concept of a Li^+ ion is therefore not a result of a charge transfer in real space, but merely a consequence of the radius assigned to the lithium atom. A direct consequence of this lack of charge transfer between the lithium and oxygen is that the change in the number of electrons for Mn is also small (Table 1). However, a considerable charge redistribution does occur *within* the manganese sphere itself, because of the transfer of e_g^b electrons to orbitals of the non-bonding t_{2g} band. As can be seen in Fig. 8, the non-bonding electrons around the manganese atoms are found closer to the nucleus in the lithiated phase than in the λ-MnO_2 phase. This rearrangement is also illustrated in Fig. 9, which shows the difference in electron density between $LiMn_2O_4$ and λ-MnO_2. From this figure, it is also seen that there is almost no difference in electron density at the lithium position. According to earlier work,[18,19] this lack of electron density at the lithium position is a consequence of a complete ionisation of the inserted lithium atoms. However, the electron density at the lithium position is very small compared to the oxygen and manganese positions (Fig. 10). If a neutral, free lithium atom were introduced at the 8a position, the electron density would be even smaller (Fig. 11).

Calculations with lithium atoms in the 8a position and using the experimentally determined coordinate for oxygen ($x=0.2632$)[7] show that the changes with respect to λ-MnO_2 are slightly more pronounced and lead to a total energy which is *ca.* 11 kJ mol^{-1} lower than for the ideal spinel. Similarly, the calculation with ordered lithium atoms in half of the 16c positions and using the ideal coordinate for oxygen ($x=1/4$) shows smaller differences compared to λ-MnO_2, and gives a

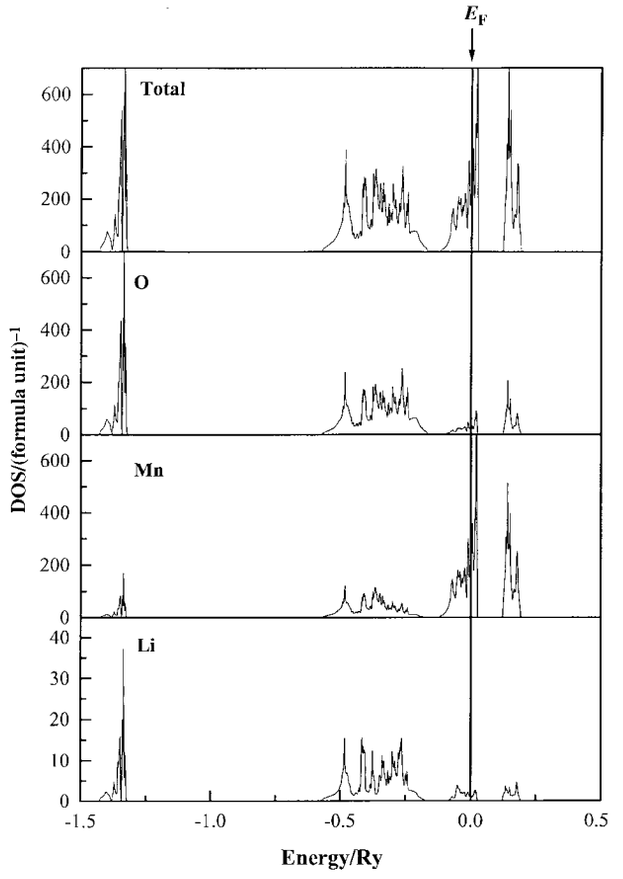

Fig. 6 The density of states (DOS) for $LiMn_2O_4$ (Li in 8a positions). The Fermi level has been shifted to zero. The DOS is given in units of number of states per formula unit and Rydberg (Ry).

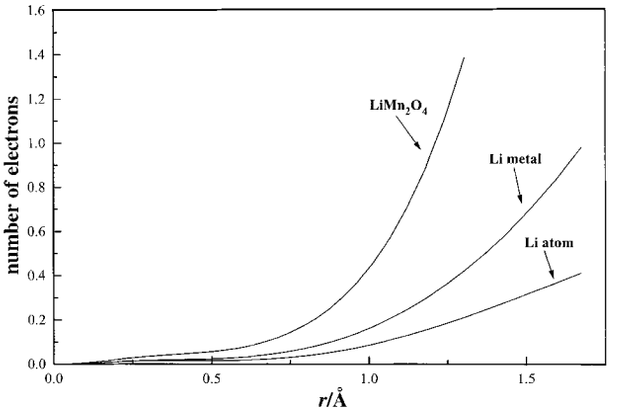

Fig. 7 The number of electrons inside a sphere of radius r for a free Li atom, Li atoms in metallic lithium and in $LiMn_2O_4$.

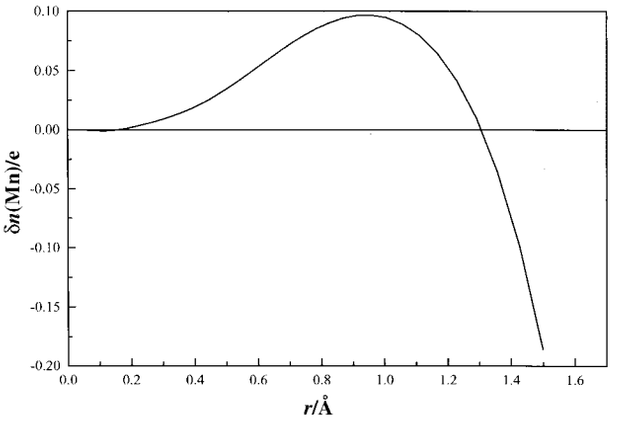

Fig. 8 The difference in the number of electrons (δn) for Mn inside a sphere of radius r for the cases of $LiMn_2O_4$ and λ-MnO_2.

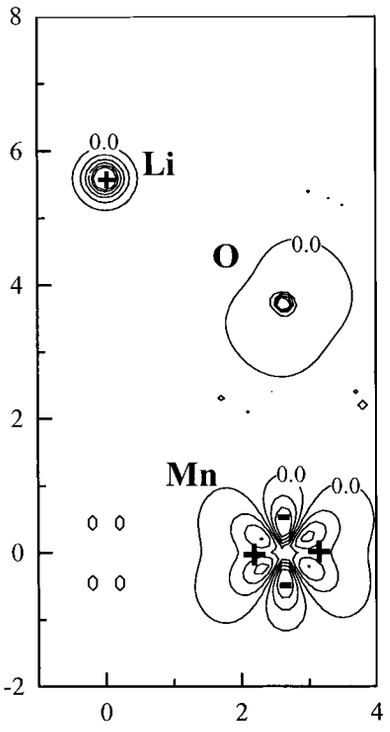

Fig. 9 The difference in electron density between $LiMn_2O_4$ and λ-MnO_2 in the cubic (1 $\bar{1}$ 0) plane. Contour interval: 0.03 $e^- a_0^{-3}$.

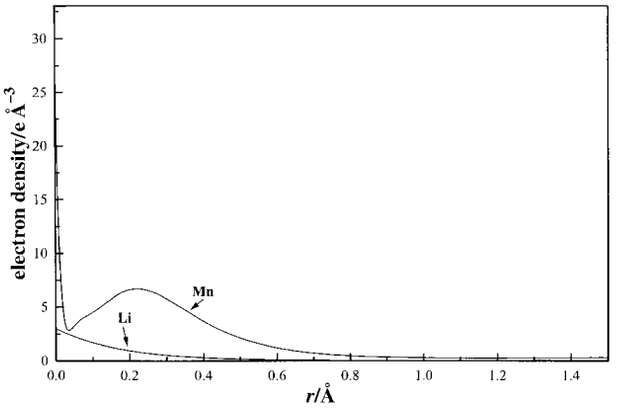

Fig. 10 The electron density for lithium and manganese in $LiMn_2O_4$ as a function of radius *r*.

total energy which is *ca.* 106 kJ mol^{-1} higher than for the ideal spinel. These calculations thus agree with the observation that lithium atoms prefer tetrahedral positions, and that the non-ideal oxygen positions stabilise the structure. The calculated lattice parameters (Table 2) are slightly smaller (1%) than those observed experimentally.

The cubic-to-tetragonal phase transition

In addition to the experimentally observed tetragonally distorted spinel structure,[10,20] calculations were also performed for two idealised hypothetical cubic structures with lithium atoms at: (i) 8a and 16c (50% occupancy) positions, and (ii) 16c positions (100% occupancy). The total DOS for the three different structural models of $Li_2Mn_2O_4$ are shown in Fig. 12. Their general shape is the same for all three models, except above the Fermi level. The band centred around *ca.* 0.1 Ry in the cubic structures is split into two bands in the tetragonal structure. This is caused by the change of coordination around the manganese ions, from an ideal MnO_6 octahedron to an elongated octahedron corresponding to a reduction in point

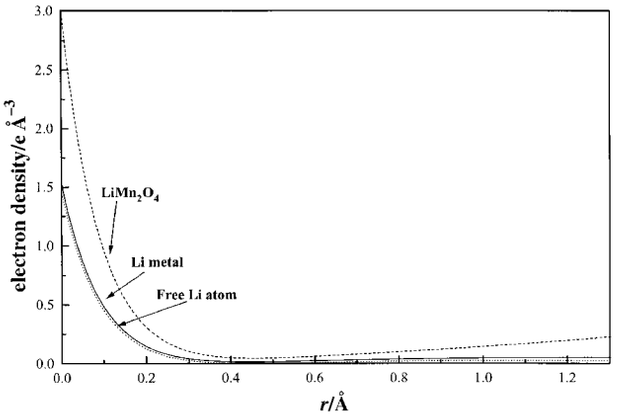

Fig. 11 The electron density for lithium in $LiMn_2O_4$, metallic lithium and a free lithium atom, as a function of distance from the nuclei.

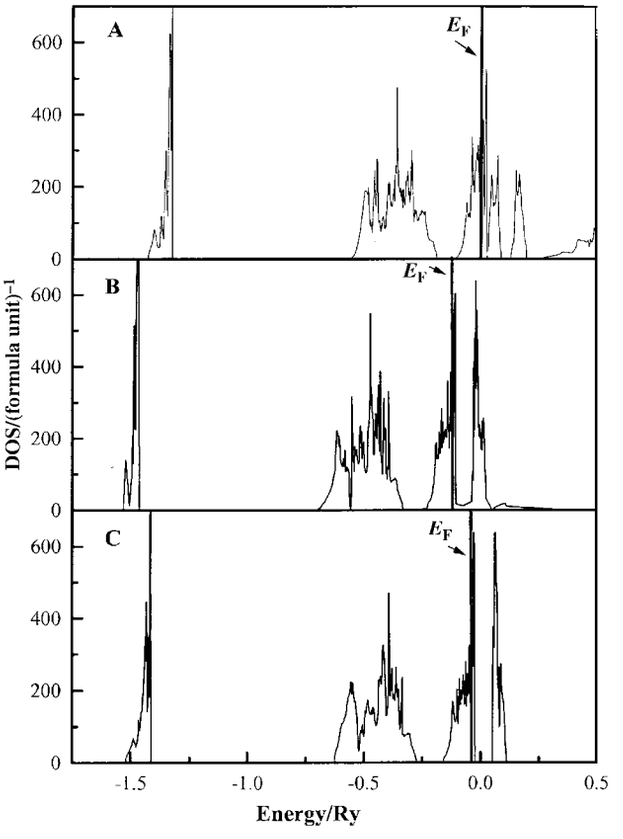

Fig. 12 Total density of states (DOS) for $Li_2Mn_2O_4$ within different structures and with lithium ions occupying different sites. The DOS is given in units of number of states per formula unit and Rydberg (Ry). The Fermi level has been shifted to zero and the unit is Ry. (A) Tetragonal structure, with Li at 4a and 8c (50% occup.) positions. (B) Cubic structure with Li at 8a and 16c (50% occup.) positions. (C) Cubic structure with Li at 16c (100% occup.) positions.

symmetry from O_h to D_{4h}. This is a consequence of the Jahn–Teller effect on the Mn^{3+} ion, and results in a splitting of the octahedral e_g and t_{2g} bands into four bands (Fig. 13).

Compared to the DOS for $LiMn_2O_4$, the bands in the DOS for the $Li_2Mn_2O_4$ model structures are slightly narrower and somewhat shifted to lower energies; the Fermi level is located at higher energies. A clear trend can be noted in these shifts: they are smallest for case (i), larger in case (ii), and largest for the case of tetragonal distortion. The total valence energy does follow the same trend, however; case (i) is the most unstable structure, while the tetragonally distorted structure is the most stable. The calculations therefore again corroborate the

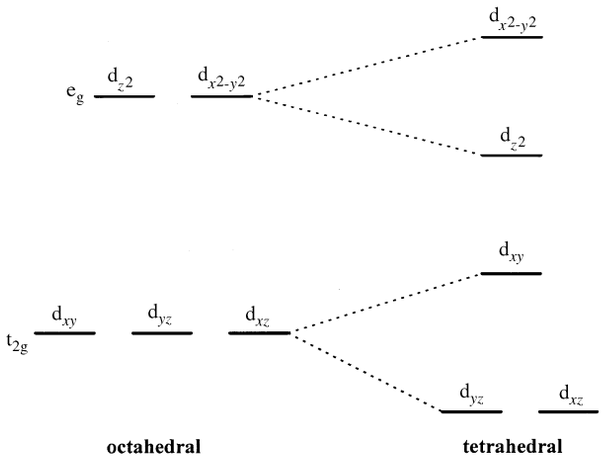

Fig. 13 A schematic representation of the splitting of d orbitals for Mn in tetragonal coordination.

experimental observation that lithium atoms are distributed in *both* tetrahedral *and* octahedral positions, and that the structure tends to favour tetragonal distortion. The cubic structure with lithium atoms at 8a and 16c (50% occupancy) positions is the most unstable structure, and is due to the close Li–Li distance.

The formation of $LiMn_2O_4$ from λ-MnO_2 by the insertion of lithium atoms results in a transfer of 0.5 electrons from manganese orbitals with a bonding e_g origin to non-bonding bands of t_{2g} character, and a corresponding transition from Mn^{4+} to $Mn^{3.5+}$. As $Li_2Mn_2O_4$ is formed on the further insertion of lithium atoms, an additional 0.5 electrons are transferred from Mn orbitals, also of bonding e_g character, to non-bonding bands of t_{2g} character; the formal Mn valency is further reduced from 3.5+ to 3+. This corresponds to an electron count of 16 in the MO model of Fig. 4a. The lattice parameters calculated for the tetragonal phase are 1% smaller (Table 2) than the experimentally observed values.[20]

The calculated stabilisation energies for the various structures are given in Fig. 14. Calculated energies of formation are given with respect to λ-MnO_2 and Li as a function of molar fraction x. The results confirm the experimental findings of the stability of the crystal structures, and also provide intercalation potentials which agree well with observations. $LiMn_2O_4$ exhibits an electrical conductivity of 1.9×10^{-5} S cm^{-1} at room temperature with an activation energy of 0.16 eV, which corresponds to an electron hopping mechanism between the two charge-states of Mn^{3+} and Mn^{4+} ions.[25]

Moreover, the spin polarisation of the manganese atoms has

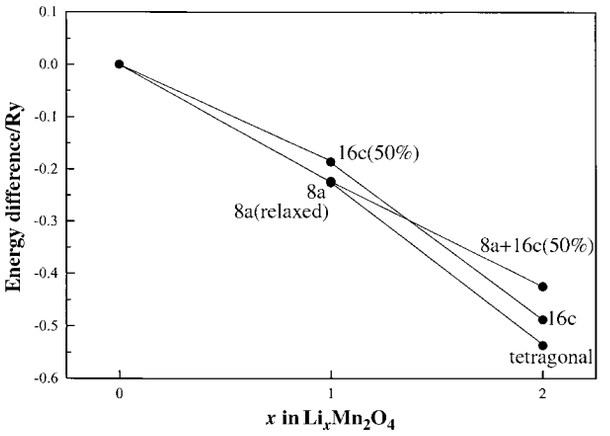

Fig. 14 The calculated energy of formation for $Li_xMn_2O_4$ as a function of x. Note: 50% stands for 50% occupation of any given position.

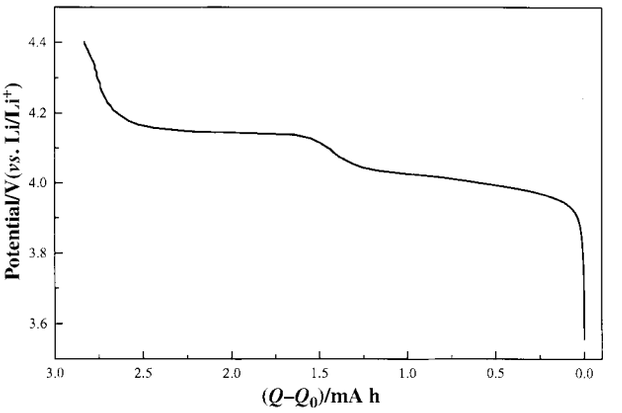

Fig. 15 Experimentally obtained discharge curve for $LiMn_2O_4$ *vs.* Li/Li^+.[26]

not been taken into account, which would cause a splitting of the t_{2g} band near the Fermi level.

Intercalation potential

The potential derived from an electrochemical cell depends on the lithium content of the cathode material. In a two-phase region of a binary section of the phase diagram, the potential is constant. For a single-phase cathode material with solid solubility, the potential usually varies slowly, but can be extreme at the ends of the solubility gap. On discharging a cell such that the electrode composition passes through a homogeneous single-phase region, the change in potential can be dramatic.

A typical discharge curve for a $<$Li|electrolyte|$LiMn_2O_4>$ cell is shown in Fig. 15. As lithium ions insert electrochemically into the λ-MnO_2 phase, the cell potential drops until the stable $LiMn_2O_4$ phase is obtained. This *change* has been calculated from eqn. (2) and (3) to be 1.51 V with Li/Li^+ as reference electrode. The total valence energy for metallic lithium in the b.c.c. lattice has been calculated as -0.282 Ry/Li, as given in Table 1. This is in reasonable agreement here with the experimental value of 1.2 ± 0.1 V. Further insertion of lithium ions into $LiMn_2O_4$ results in the transformation to the tetragonal $Li_2Mn_2O_4$ phase; the corresponding *change* has here been calculated as 1.16 V, again in agreement with the experimental value of 1.1 ± 0.1 V.[20] If Jahn–Teller distortion of the cubic structure were not taken into account, the change in potential would be 0.49 V for lithium atoms going only into 16c positions. For lithium atoms going into both 8a and 16c positions, a potential increase by a further 0.37 V was obtained. We thus see that Jahn–Teller distortion plays a vital rôle in the stabilisation of the $Li_2Mn_2O_4$ phase, and (contrary to earlier beliefs[19]) cannot be neglected.

Conclusions

An LMTO-ASA approach has shown that the main effect of lithium insertion into a λ-MnO_2 host structure is the replacement of Mn orbitals with e_g character in the bonding band by lithium orbitals of s and p character. The Mn electrons are promoted into the non-bonding t_{2g} level, resulting in the corresponding reduction in formal charge on the Mn atom. All charge-transfer effects between different atom types are small, whereas the charge redistribution within the Mn atoms is substantial. The calculated stabilities for the various structural alternatives provide a clear explanation of the experimental observations. Moreover, the Jahn–Teller distortion is shown to play a crucial rôle in the stabilisation of the $Li_2Mn_2O_4$ phase; this has not been demonstrated previously.

Acknowledgements

This work has been supported by grants from The Swedish Natural Science Research Council (NFR), The Swedish Board for Technical Development (NUTEK) and the EU (Joule III) Non-Nuclear Energy Sources Programme. All are hereby gratefully acknowledged.

References

1 M. G. S. R. Thomas, W. I. F. David, J. B. Goodenough and P. Groves, *Mater. Res. Bull.*, 1985, **20**, 1137.
2 C. Delmas, H. Cognac-Auradon, J. M. Cocciantelli, M. Ménétrier and J. P. Doumerc, *Solid State Ionics*, 1994, **69**, 257.
3 Ö. Bergström, *Comprehensive Summaries of Uppsala Dissertations from the Faculty of Science and Technology*, No. 336, Uppsala University, 1998.
4 A. R. Armstrong and P. G. Bruce, *Nature (London)*, 1996, **381**, 499.
5 M. Broussely, F. Perton, J. Labat, R. J. Staniewicz and A. Romero, *J. Power Sources*, 1993, **43–44**, 209.
6 Y. Gao and J. R. Dahn, *J. Electrochem. Soc.*, 1996, **143**, 100.
7 H. Berg, W. Liu, G. C. Farrington and J. O. Thomas, *Solid State Ionics*, 1998, **112**, 167.
8 G. Pistoia and G. Wang, *Solid State Ionics*, 1993, **66**, 135.
9 M. M. Thackeray, A. de Kock, M. H. Rossouw, D. Liles, R. Bittihn and D. Hoge, *J. Electrochem. Soc.*, 1992, **139**, 363.
10 T. Ohzuku, M. Kitagawa and T. Hirai, *J. Electrochem. Soc.*, 1990, **137**, 769.
11 W. Y. Liang, *Microionics—Solid State Integrable Batteries*, ed. M. Balkanski, North-Holland, Amsterdam, 1991, pp. 237–251.
12 C. Julien and M. Balkanski, *Solid State Ionics III*, ed. G. A. Nazri, J. M. Tarascon and M. Armand, MRS Symposium Proceedings No. 293, Materials Research Society, Pittsburgh, PA, 1993, pp. 27–37.
13 J. Friedel, *Adv. Phys.*, 1954, **3**, 446.
14 D. J. Sellmeyer, *Solid State Physics: Advances in Research and Applications*, ed. H. Ehrenreich, F. Seitz and D. Turnbull, Academic, New York, 1978, vol. 33, p. 83.
15 J. V. McCanny, *J. Phys. C*, 1979, **12**, 3263.
16 C. Umrigar, D. E. Ellis, D. S. Wang, H. Krakauer and M. Posternak, *Phys. Rev. B*, 1982, **26**, 4935.
17 G. Y. Guo and W. Y. Liang, *J. Phys. C*, 1987, **20**, 4315.
18 M. K. Aydinol, A. F. Kohan, G. Ceder, K. Cho and J. Joannopoulos, *Phys. Rev. B*, 1997, **56**, 1354.
19 M. K. Aydinol and G. Ceder, *J. Electrochem. Soc.*, 1997, **144**, 3832.
20 M. M. Thackeray, W. I. F. David, P. G. Bruce and J. B. Goodenough, *Mater. Res. Bull.*, 1983, **18**, 461.
21 J. C. Hunter, *J. Solid State Chem.*, 1981, **39**, 142.
22 O. K. Andersen, *Phys. Rev. B*, 1975, **12**, 3060.
23 H. L. Skriver, *The LMTO Method*, Springer Series in Solid State Science, vol. 41, Springer, Berlin, 1984.
24 R. D. Shannon and C. T. Prewitt, *Acta Crystallogr., Sect. B.*, 1969, **25**, 925.
25 S. Chitra, P. Kalyani, T. Mohan, M. Massot, S. Ziolkiewicz, R. Ganganharan, M. Eddrief and C. Julien, *Ionics*, 1998, **4**, 8.
26 H. Berg and J. O. Thomas, *Solid State Ionics*, in press.

Paper 9/05575D